International Journal of Chemical Studies

P-ISSN: 2349–8528
E-ISSN: 2321–4902
IJCS 2017; 5(6): 1954-1960

Received: 28-09-2017
Accepted: 29-10-2017

Meigui Feng
College of Chemistry and Environmental Science, Hebei University, Baoding 071002, China

Dongxia An
College of Chemistry and Environmental Science, Hebei University, Baoding 071002, China

Hong Zhang
College of Chemistry and Environmental Science, Hebei University, Baoding 071002, China

Gang Ma
College of Chemistry and Environmental Science, Hebei University, Baoding 071002, China

Cuimiao Zhang
College of Chemistry and Environmental Science, Hebei University, Baoding 071002, China

Zhiguang Ma
(1) College of Chemistry and Environmental Science, Hebei University, Baoding 071002, China
(2) Key Laboratory of Chemical Biology of Hebei Province, Hebei University, Baoding 071002, China

Correspondence
Zhiguang Ma
(1) College of Chemistry and Environmental Science, Hebei University, Baoding 071002, China
(2) Key Laboratory of Chemical Biology of Hebei Province, Hebei University, Baoding 071002, China

Facile synthesis of cobalt/nickel tungstate and its application in hybrid supercapacitor

Meigui Feng, Dongxia An, Hong Zhang, Gang Ma, Cuimiao Zhang and Zhiguang Ma

Abstract
In this paper, cobalt/nickel tungstate materials ($CoWO_4$@$NiWO_4$-A) have been synthetized by co-precipitation in alkaline condition, and the electrochemical behaviors of the samples were investigated. The as-prepared composites have been systematically characterized by powder X-ray diffraction, scanning electron microscopy, and Brunauer-Emmett-Teller analysis. The pseudocapacitive performances of composite electrode materials were investigated by the electrochemical tests. The $CoWO_4$@$NiWO_4$-A showed good electrochemical performances. In addition, a hybrid supercapacitor (HSC) was assembled by using the $CoWO_4$@$NiWO_4$-A as the positive electrode and activated carbon (AC) as negative electrode. The HSC exhibited an energy density of 11.96 Wh/kg at a power density of 1090 W/kg. In addition, the HSC displayed good cyclic stability after 5000 continuous charge-discharge tests. Therefore, this work provides a candidate electrode materials for supercapacitors.

Keywords: Supercapacitors, electrode material, co-precipitation, cobalt/nickel tungstates

1. Introduction
In the twenty-first century, mankind faced enormous challenges in energy crisis and environmental protection. Due to the use of coal and fossil fuel, the pollution is getting worse and the fossil fuels are drying up. Therefore, scientists are devoted to the invention of new renewable energy storage devices. Supercapacitors, also known as electrochemical capacitors (ECs) have features of high energy density and power density, fast charge-discharge rate, excellent cycle stability and environmental safety [1, 2]. Hence, the ECs have many applications in electronics, national defense, communication, vehicle, aviation and so on. Supercapacitors are classified into two groups by the energy storage theory: (i) electrochemical double layer capacitors (EDLCs), which store energy by the double layer of electrode-electrolyte interface [3]. Various carbon-based materials have been used as the electrode materials of the EDLCs due to large specific area, abundant pore structure and favorable conductivity [4]; (ii) Faradic pseudocapacitors, based on the rapid Faradic redox reaction of the electrode materials [5], such as metal oxides/hydroxides [6] and conducting polymers [7].
At present, many researchers are developing various novel electro-active materials with low cost, high electrochemical properties and environmental safety [6]. Transition metal oxides and other composites have been widely applied in electrode materials of pesudocapacitors owing to their diverse oxidation states, good conductivity and high capacitance. These materials include the oxides of Ru [8], Ni [9], Co [10], V [11], Fe [12], and so on. In addition, transition metal tungstate composites not only have been used for luminescent materials, pigments, catalyst and sensors, but also have been applied in electrochemistry for storage devices. Recently, more researchers are devoted to study the electrochemical performances of metal tungstate compounds, such as 3D nanoporous $ZnWO_4$ [13], $NiCo_2O_4$@$NiWO_4$ [14], $CoWO_4$ [15], $FeWO_4$ [16], RGO/$CoWO_4$ [17], $NiWO_4$/reduced graphene oxide [18], Co_3O_4@$CoWO_4$/rGO [19], and so on. It indicated that metal tungstate composites are promising candidates of electro-active materials.
In this article, we prepared cobalt and nickel tungstate composites ($CoWO_4$, $NiWO_4$, $CoWO_4$@$NiWO_4$ and $CoWO_4$@$NiWO_4$-A) by a facile chemical co-precipitation method, and their electrochemical performances were compared by the cyclic voltammetry (CV), galvanostatic charge-discharge (GCD) and electrochemical impedance spectroscopy (EIS). It is found that $CoWO_4$@$NiWO_4$-A as an electrode material has better electrochemical performance. In addition, a hybrid supercapacitor $CoWO_4$@$NiWO_4$-A//AC was assembled successfully and its electrochemical performances were evaluated.

2. Experimental

2.1 Synthesis of $CoWO_4$@$NiWO_4$-A

All reagents in the experiment were of analytical grade and directly used without any purification. $CoWO_4$@$NiWO_4$-A powders were prepared by carrying out the reaction between $NaWO_4 \cdot 2H_2O$ and sulfates in a flask under magnetic stirring. In a typical synthesis, first, 2.5 mmol sulfates ($NiSO_4 \cdot 6H_2O$: $CoSO_4 \cdot 7H_2O$ = 3:1, molar ratio) were dissolved in 25 mL ultrapure water under magnetic stirring and further stirred for about 30 min at room temperature (solution A). Next, 1.25 mmol $Na_2WO_4 \cdot 2H_2O$ and 1.25 mmol NaOH were dissolved in 25 mL ultrapure water under magnetic stirring (solution B). Finally, the solution B was added dropwise into the solution A under magnetic stirring, and then the resulting suspension was further stirred for 3h. The obtained precipitate was separated by centrifugation, washed with abundant ultrapure water and ethanol for several times, and dried at 60 °C in vacuum for 12 h.

For comparison, $CoWO_4$, $NiWO_4$ and $CoWO_4$@$NiWO_4$ prepared through a similar route as for $CoWO_4$@$NiWO_4$-A. For $CoWO_4$@$NiWO_4$, a solution B was added dropwise into a solution A under stirring, except that NaOH was not used in solution B, and the amount of substance of WO_4^{2-} in the solution B is 2.5 mmol. For the $CoWO_4$ and $NiWO_4$, the solution containing 2.5 mmol $Na_2WO_4 \cdot 2H_2O$ was added dropwise into the solution containing equimolar of $CoSO_4 \cdot 7H_2O$ under stirring, and the $NiWO_4$ prepared through a similar route as for $CoWO_4$. The similar processes were repeated to get $CoWO_4$, $NiWO_4$ and $CoWO_4$@$NiWO_4$ powders.

2.2 Materials characterization

The morphologies of the as-prepared products were observed by field emission scanning electron microscope (SEM, JSM-7500F). The crystal structures and compositions of the as-prepared samples were characterized by X-ray powder diffraction (XRD, Bruker D8 Advance). N_2 absorption-desorption were performed with a Micromeritics Tristar Ⅱ 3020. The surface area was computed from the Brunauer–Emmett-Teller (BET) equation, and the pore size distribution was calculated from the desorption curve by the Barrette-Joynere-Halenda (BJH) model.

2.3 Electrochemical measurements

The electrochemical measurements were investigated on an electrochemical workstation (Interface 1000, Gamry Instruments, USA) using a three-electrode system. The reference electrode was a saturated calomel electrode (SCE), and the counter electrode was a platinum plate. The working electrodes were prepared as follows: the as-prepared electro-active materials, acetylene black and polytetrafluoroethylene (PTFE) concentrated dispersion (10 wt.%) were mixed together in a mass ratio of 80:15:5 with absolute ethanol to form homogeneous mixture slurry. The slurry coated on the pre-cleaned nickel foam support (1 cm×1 cm) and then dried at 60 °C in vacuum for 12 h. Finally, the prepared electrode was pressed at 10 MPa. The AC electrode was fabricated in the same way. The mass loading of active materials for the electrode is about 3 mg.

The electrochemical tests were carried out using 1 M KOH aqueous solution as the electrolyte. The electrochemical performances of the prepared electrodes were tested by CV, GCD and EIS measurements. The EIS measurements were carried out in the frequency range of 100 kHz to 0.01 Hz at the open circuit potentials, and the applied potential amplitude was 5 mV. The corresponding specific capacitance(C) was calculated from the following equations:

$$C = \frac{I\Delta t}{m\Delta V} \quad (1)$$

in which C is the specific capacitance (F/g), I is the discharge current (A), t is the discharge time (s), V is the potential window (V), m is the mass of electro-active materials in the electrodes (g).

3. Results and discussion

3.1 The structural and morphological characterization of samples

Fig 1. shows the XRD patterns of the as-prepared samples. Evidently, the powders of samples were amorphous without any crystallized phases. In other words, the broad diffraction peaks with low intensity should result from the amorphous state and/or nanometer-scale size of the as-prepared samples [20]. This phenomenon is corresponding to previous reports on $CoWO_4$-$NiWO_4$, $CoWO_4$ and $NiWO_4$ [20-22]. In addition, there is no peak from $Co(OH)_2$ and $Ni(OH)_2$ in the patterns, which is attributed to slight $Co(OH)_2$ and $Ni(OH)_2$ in the samples.

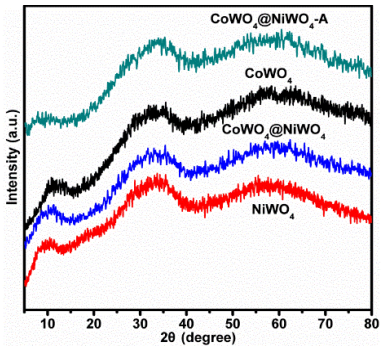

Fig 1: XRD patterns of the metal tungstates.

Fig 2. Displays FT-IR spectrum for the fabricated ($CoWO_4$, $NiWO_4$, $CoWO_4$@$NiWO_4$, $CoWO_4$@$NiWO_4$-A) powders recorded within 4000-400 cm^{-1} range. The absorption bands at about 3400 cm^{-1} and 1630 cm^{-1} refer to –OH stretching and bending vibration of the water absorption. The characteristic stretching absorption bands of metal tungstate range from 950 cm^{-1} to 400 cm^{-1} [23]. It is obviously that the weak absorption bands with the maxima at 835-850 cm^{-1} can be contributed to the stretching mode of W-O bonds in the joints with WO_4 tetrahedral [24]. The bands at about 930 cm^{-1} corresponds to the stretching mode of the W=O bond [25]. The weak bands at 680 cm^{-1} is caused by the asymmetric stretching vibration of O-W-O bridges [15]. All of results further confirm that the synthesized amorphous materials are tungstate composites.

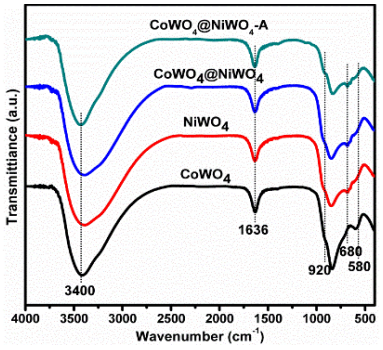

Fig 2: FT-IR spectra of $CoWO_4$, $NiWO_4$, $CoWO_4$@$NiWO_4$ and $CoWO_4$@$NiWO_4$-A.

The morphology characters of $CoWO_4$, $NiWO_4$, $CoWO_4$@$NiWO_4$ and $CoWO_4$@$NiWO_4$-A are shown in Fig 3a-d. The images were got under the same magnification. As observed from SEM images (Fig 3a-d), the as-prepared samples are made up of wafer-like architecture, and the particles are randomly assembled and aggregated together. In addition, the particle size of $CoWO_4$@$NiWO_4$-A was smaller than other as-prepared samples, indicating the sample possesses higher specific area. The smaller size can shorten the path length of ion transfer and drastically enhance the charge-discharge rate [26].

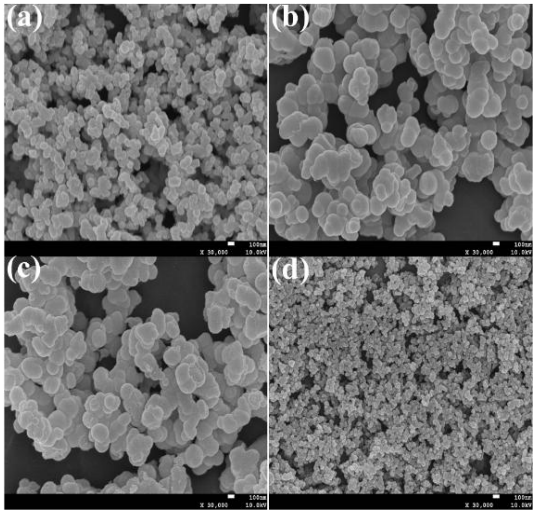

Fig 3: SEM images of the metal tungstates: (a) $CoWO_4$, (b) $NiWO_4$, (c) $CoWO_4$@$NiWO_4$, (d) $CoWO_4$@$NiWO_4$-A.

The surface area and pore structure of $CoWO_4$@$NiWO_4$ and $CoWO_4$@$NiWO_4$-A were measured by the nitrogen adsorption and desorption experiments as shown in Fig 4. The samples show a typical IV isotherm profile with distinct hysteresis loops. The Brunauer-Emmett-Teller (BET) specific surface area for $CoWO_4$@$NiWO_4$ and $CoWO_4$@$NiWO_4$-A materials are 6.97, 72.62 m^2/g, with the total pore volume of 0.02, 0.19 cm^3/g, respectively. The surface area of the $CoWO_4$@$NiWO_4$-A is higher than that of the $CoWO_4$@$NiWO_4$. Hence, $CoWO_4$@$NiWO_4$-A exhibits the larger electro-active surface area and higher electrochemical performances. The $CoWO_4$@$NiWO_4$ and $CoWO_4$@$NiWO_4$-A exhibit mesoporous structure with average pore size of 10.1 nm and 9.1 nm, respectively. The mesoporous structures are approachable to electrolyte ions and facilitate the charge accumulation and fast charge transfer, resulting in the improved specific capacitance and rate capability [27].

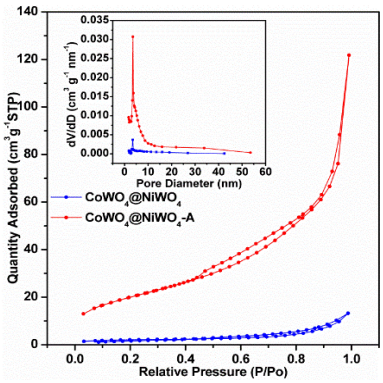

Fig 4: Nitrogen adsorption-desorption isotherms of $CoWO_4$@$NiWO_4$ and $CoWO_4$@$NiWO_4$-A. The inset shows its pore size distribution plot.

3.2 Electrochemical characterization

3.2.1 Electrochemical performances of samples

Fig 5. Depicts the CV curves of the $CoWO_4$, $NiWO_4$, $CoWO_4$@$NiWO_4$ and $CoWO_4$@$NiWO_4$-A under the same scanning rate (5 mV/s) in the potential range from 0 to 0.55 V. As we have seen, CV curve of each sample exhibits a pair of redox peaks, indicating typical pseudocapacitive properties. The observed redox peaks are owing to the charge-transfer kinetics of Co^{2+}/Co^{3+} and Ni^{2+}/Ni^{3+} in the metal tungstates. The electrochemical reactions are as follows [28]:

$$Co(OH)_2 + OH^- \rightleftharpoons CoOOH + H_2O + e^- \quad (2)$$

$$Ni(OH)_2 + OH^- \rightleftharpoons NiOOH + H_2O + e^- \quad (3)$$

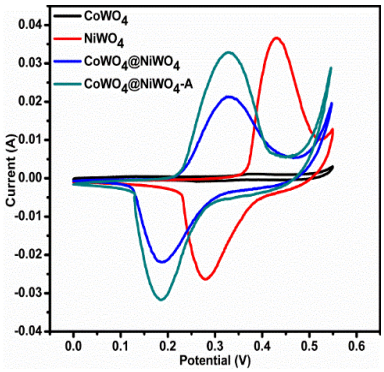

Fig 5: CV curves of the as-prepared electrodes at 5 mV/s.

It is found that integral area of $CoWO_4$@$NiWO_4$-A is ultimate, which maybe indicates its higher specific capacitances. Fig 6. Shows the CV curves of $CoWO_4$@$NiWO_4$-A at various scan rates. Obviously, all the curves exhibit a pair of strong redox peaks in the range of 0.1-0.2 V and 0.3-0.4 V, indicating typical faradic pseudocapacitive behavior, which is ascribed to the quasi-reversible reaction between Ni^{2+}/Ni^{3+} and Co^{2+}/Co^{3+} [29]. The redox peaks of CV curves become wider with the increasing scan rates from 5 to 50 mV/s, and the anodic peak potential shifts positively, meanwhile, the cathodic peak potential shifts negatively [30]. Nonetheless, the CV curves still display a pair of redox shape at a sweep rate of 50 mV/s, suggesting that tungstates electrodes were beneficial to fast redox reactions.

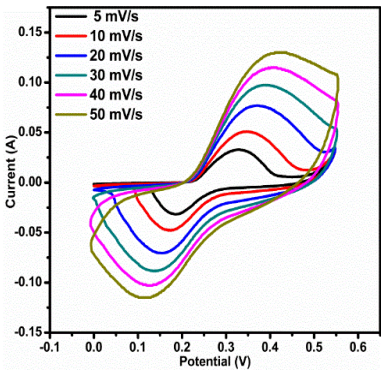

Fig 6. CV curves of $CoWO_4$@$NiWO_4$-A electrode at various scan rates.

In order to further investigate the specific capacitance, GCD tests were carrying out in 1M KOH within a potential range from 0 to 0.48 V. Fig 7. Presents the charge-discharge curves of as-prepared samples at a current density of 1 A/g. The $CoWO_4$@$NiWO_4$-A exhibits a specific capacitance as high as 677.5 F/g for the first discharge, and the specific capacitances calculated from Eq. (1) for $CoWO_4$, $NiWO_4$ and

$CoWO_4$@$NiWO_4$ are 36.2, 433.3 and 493.1 F/g, respectively. Obviously, $CoWO_4$@$NiWO_4$-A has the highest specific capacitance, which is owing to the fast intercalation/de-intercalation of electrolyte ions via active sites of electrode material and the generation of slight $Co_{0.25}Ni_{0.75}(OH)_2$. It exhibited that the composites have better electrochemical properties in alkaline. Fig 8. exhibits the galvanostatic charge-discharge curves of $CoWO_4$@$NiWO_4$-A electrode within a potential range from 0 to 0.48 V at different current densities. According to the Eq. (1), the specific capacitance for the first discharge of $CoWO_4$@$NiWO_4$-A are calculated to be 677.5, 641.7, 622.3, 593.8, 548 and 515 F/g at current densities of 1, 2, 3, 5, 8 and 10 A/g, respectively. The good rate capability is ascribed to the good conductivity of the electrode material and small charge transfer resistance.

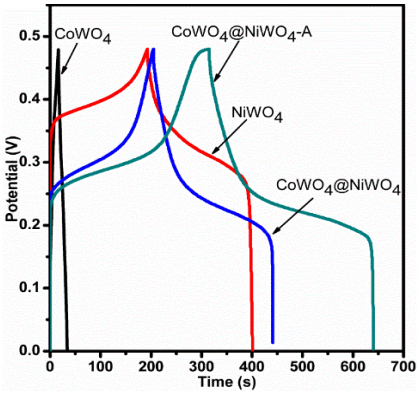

Fig 7: Galvanostatic charge-discharge curves of as-prepared electrodes at a current density of 1 A/g.

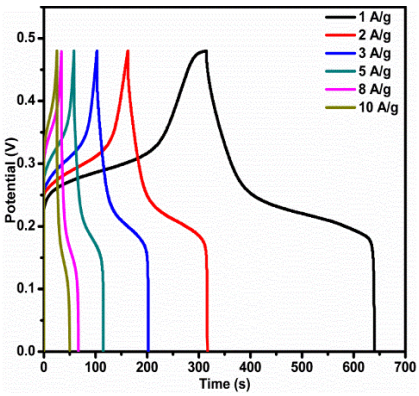

Fig 8: Charge-discharge curves of the $CoWO_4$@$NiWO_4$-A electrode at different current density.

Fig 9. demonstrates the specific capacitance *vs.* current density curves for $NiWO_4$, $CoWO_4$@$NiWO_4$ and $CoWO_4$@$NiWO_4$-A electrodes. It displays that the specific capacitance of all the samples decreases with increasing of the current density, which might be due to the circuitous diffusion of OH^- ions into the pores of the electrode materials as well as the electrode resistance [31, 32]. The specific capacitance of $CoWO_4$@$NiWO_4$-A for the first discharge still maintains 76% of initial specific capacitance when the current density increases from 1 A/g to 10 A/g. However, the rate capabilities of $NiWO_4$ and $CoWO_4$@$NiWO_4$ are 42% and 64%, respectively. The cyclic stability is a crucial factor to investigate the electrochemical performances of the electro-active materials. The calculated retentions of as-prepared samples were shown in the Fig 10. in a voltage window from 0 to 0.48 V at a current density of 5 A/g. It was clearly seen that the capacitance of $CoWO_4$@$NiWO_4$-A increased in the first 50 cycles, possibly owing to the activation of electrode materials. The $CoWO_4$@$NiWO_4$-A exhibits better capacitance retention of 80% than other reported samples (the retention rates of $NiWO_4$ and $CoWO_4$@$NiWO_4$ are 29% and 74%, respectively), demonstrating its good electrochemical stability.

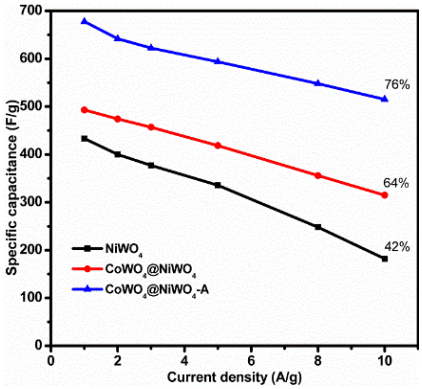

Fig 9: Specific capacitance of the as-prepared electrodes at different current densities.

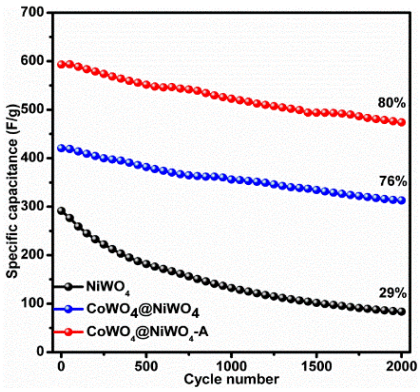

Fig 10: Cycling stability of the as-prepared electrodes at 5 A/g.

In order to further investigate the performance and impedance of the electrode materials, EIS measurements were performed. Fig 11. displays the typical Nyquist plots of $CoWO_4$, $NiWO_4$, $CoWO_4$@$NiWO_4$ and $CoWO_4$@$NiWO_4$-A compounds. The corresponding equivalent circuit model that applied to fit the EIS data is given in the inset of Fig 11. All the Nyquist plots are similar, being made up of a semicircle at the high-frequency region, a linear section at the low-frequency region and a transition zone between two regions. At the high-frequency region, the semicircle diameter of Nyquist plot corresponds to the interfacial charge-transfer resistance (R_{ct}) occurring at the electrode/electrolyte interface and double layer capacitance, which is mainly associated with the Faradaic reactions. The internal resistance (R_s) obtained from the intercept of the plots on the real axis, which mainly includes ion impedance of electrolyte, intrinsic impendence of the electrode materials and contact resistance between active materials and current collectors [21]. In the low-frequency region, the almost straight line of the slope of 45° is referred to as the Warburg resistance (W), which corresponding to the ion diffusion in the host material diffusive resistance of the electrolyte in the electrode surface [33]. The measured impedance spectra of samples were further analyzed based on the equivalent circuit. The constant phase angle element Φ_1 and Φ_2 represent non-ideal capacitive behavior [34]. The fitted values are listed in Table 1. As shown in the Table 1, the R_{ct} of $CoWO_4$@$NiWO_4$-A electrode material is lower than pure

$NiWO_4$ and $CoWO_4$@$NiWO_4$ compound, indicating that $CoWO_4$@$NiWO_4$-A has faster charge-transfer, which can enhance the electrochemical properties of the electrode material. It is corresponding to the results of the previous CV and GCD.

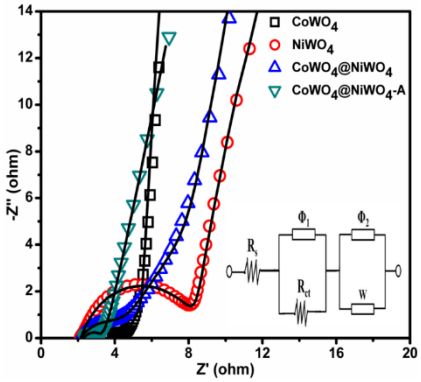

Fig 11: Nyquist plots of the as-prepared electrodes. The inset shows the electrical equivalent circuit used for fitting impedance spectra.

Table 1: The fitted values of R_s and R_{ct} of as-prepared electrodes based on the equivalent circuit.

	R_s (Ω)	R_{ct} (Ω)
$CoWO_4$	3.855	0.835
$NiWO_4$	2.159	6.243
$CoWO_4$@$NiWO_4$	2.131	2.525
$CoWO_4$@$NiWO_4$-A	2.309	1.108

3.2.2 Electrochemical property of the hybrid supercapacitor

The $CoWO_4$@$NiWO_4$-A//AC aqueous hybrid supercapacitor was fabricated by using of $CoWO_4$@$NiWO_4$-A and AC as positive and negative electrodes, respectively. As for a capacitor, the charge balance between two electrodes follows the relationship according to equation [35]:

$$C_+ m_+ \Delta V_+ = C_- m_- \Delta V_- \quad (4)$$

Where C (F/g) is the specific capacitance, m (g) is the mass of the active material in the electrode, ΔV (V) is the voltage window. On the basis of the charge-discharge test, the specific capacitance of $CoWO_4$@$NiWO_4$-A and AC electrode is 677.5 and 146 F/g at a discharge current density of 1 A/g. According to the Eq. (4), the optimal mass ratio of the active materials expected to be m (AC)/m[$CoWO_4$@$NiWO_4$-A] = 2.2 in the hybrid capacitor. In this article, the weight of active materials of positive and negative electrode is 2.4 mg and 5.3 mg, respectively. Electrochemical performance of the HSC was characterized by CV and GCD measurements.

Fig 12. demonstrates the CV curves of the activated carbon and $CoWO_4$@$NiWO_4$-A in 1 M KOH aqueous solution at 5 mV/s. According to the figure, activated carbon demonstrates the typical rectangular shape from -1.0 to 0 V at a scan rate of 5 mV/s. The $CoWO_4$@$NiWO_4$-A material exhibits a pair of redox peaks with a stable potential window of 0-0.55 V as a faradaic positive electrode. Consequently, the cell voltage can be extended up to 1.48 V. Fig 13. shows the CV curves of the $CoWO_4$@$NiWO_4$-A//AC HSC at various scan rates between 0 and 1.48 V. The CV curves demonstrated a larger current area with broader redox peak when the scan rate increased from 5 to 50 mV/s, which indicate pseudocapacitive behavior of $CoWO_4$@$NiWO_4$-A//AC HSC.

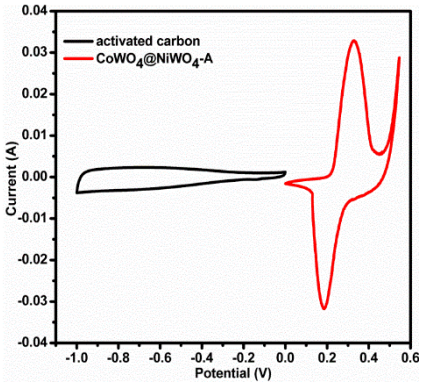

Fig 12: CV curves of $CoWO_4$@$NiWO_4$-A and activated carbon (AC) electrodes at a scan rate of 5 mV/s.

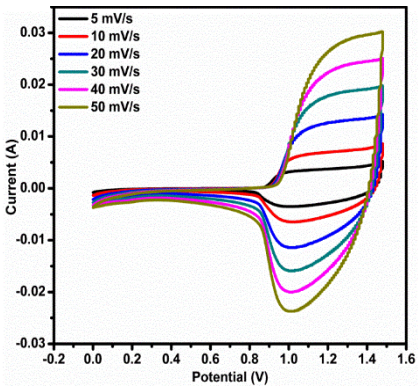

Fig 13: CV curves of the hybrid supercapacitor $CoWO_4$@$NiWO_4$-A//AC at various scan rates.

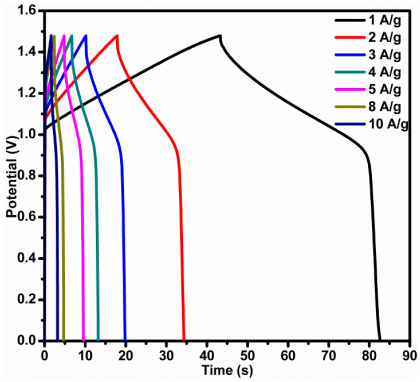

Fig 14: Galvanostatic charge-discharge curves of $CoWO_4$@$NiWO_4$-A//AC with a potential of 1.48 V at various current densities.

GCD curves of HSC at different current densities are shown in Fig 14. The specific capacitance of HSC was calculated from GCD curves according to Eq. (1). It should be noted that m (g) means the total mass of the active material in the positive and negative electrodes. The calculated specific capacitance values are 26.60, 22.26, 19.61, 17.59, 15.99, 12.51 and 10.76 F/g at current densities of 1, 2, 3, 4, 5, 8 and 10 A/g, respectively. In addition, the energy densities and power densities of the Ragone plot is a key curve to characterize the performance of electrochemical supercapacitors. The corresponding relationship between energy densities (E, Wh/kg) and power densities (P, W/kg) of the HSC can be calculated from the following equations [36]:

$$E = \frac{\int_0^t IV(t)dt}{m} \quad (5)$$

$$P = \frac{E}{\Delta t} \quad (6)$$

Where I (A) is the discharge current, V (V) is the potential range during galvanostatic discharge process, Δt (s) is the discharge time and m (g) is the total mass of active material of electrodes. The Ragone plot showing the relationship between energy densities and power densities of the asymmetric device is shown in Fig 15. The maximum energy density of the HSC was recorded as 11.96 Wh/kg with a corresponding power density of 1.09 kW/kg. In addition, the device maintains 3.97 Wh/kg with a high power density of 8.97 kW/kg. Some previous reported supercapacitors based on tungstates were fabricated and tested. For instance, Ma *et al*. assembled the CBC-1//$K_{0.3}WO_3$ ASC, which exhibited an energy density of 26.3Wh/kg corresponding power density of 404.2 W/kg [37], Wang *et al*. prepared the $NiWO_4$-$CoWO_4$//AC hybrid supercapacitor, which showed an energy density of 30.1 Wh/kg at a power density of 200 W/kg [21]. The inset of Fig 15. shows the HSC can light a lamp for about 15 seconds.

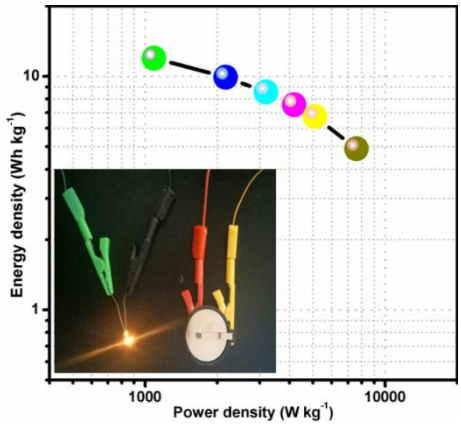

Fig 15: Ragone plot of the $CoWO_4$@$NiWO_4$-A//AC, the inset shows the application of the hybrid supercapacitor.

Fig 16. Exhibits the cycling stability and coulombic efficiency of $CoWO_4$@$NiWO_4$-A//AC within the potential range of 0-1.48 V at the current density of 5 A/g. The HSC exhibits better cyclic stability with 82% of the initial capacitance after 5000 continuous galvanostatic charge-discharge cycling experiments. In addition, the coulombic efficiency maintains about 79% during first few cycles, while it maintains 100% during next cyclic experiments, which is ascribed to activation of electrode materials. The cycling performance of HSC indicates that it has good electrochemical stability.

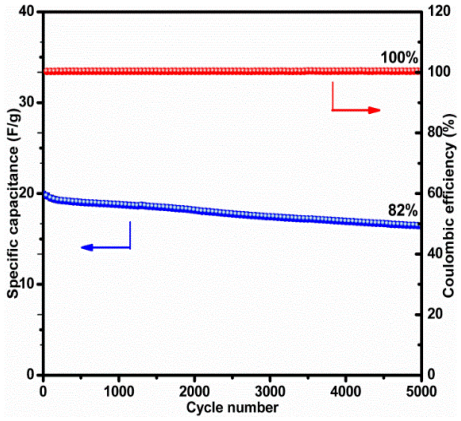

Fig 16: Cycling stability and coulombic efficiency of $CoWO_4$@$NiWO_4$-A//AC within the potential range of 0-1.48 V at the current density of 5 A/g.

4. Conclusion

In summary, we have presented a facile approach to prepare the metal tungstate ($CoWO_4$@$NiWO_4$-A) by chemical co-precipitation method. The $CoWO_4$@$NiWO_4$-A electrode shows good electrochemical performance, with a high specific capacitance of 677.5 F/g at 1 A/g and desirable cyclic stability. For its practical application, a hybrid supercapacitor $CoWO_4$@$NiWO_4$-A//AC was assembled, the electrochemical performance of the device was investigated within a potential range of 0-1.48 V and exhibits good capacitance property. The HSC shows better cycling stability with 82% capacitance retention over 5000 cycles at 5 A/g. All above results demonstrated that metal tungstate materials could be considered as promising electrode materials for pseudocapacitors in energy storage systems.

Acknowledgements

We gratefully thank the financial support from Program for National Natural Science Foundation of China (51302062).

References

1. Bouroushian M, Karoussos D, Kosanovic T, Conway BE. Electrochemical Supercapacitors: Scientific Fundamentals and Technological Applications, Kluwer Academic/ Plenum Publisher, New York, 1999.
2. Simon P, Gogotsi Y. Materials for electrochemical capacitors. Nature Materials. 2008; 7(11):845-854.
3. Pandolfo AG, Hollenkamp AF. Carbon properties and their role in supercapacitors. J Power Sources. 2006; 157(1):11-27.
4. Li M, Zhang YQ, Yang LL, Liu YK, Ma JY. Excellent electrochemical performance of homogeneous polypyrrole/graphene composites as electrode material for supercapacitors. Journal of Materials Science-Materials in Electronics. 2015; 26(1):485-492.
5. Zhang H, Cao G, Yang Y. Carbon nanotube arrays and their composites for electrochemical capacitors and lithium-ion batteries. Energy & Environmental Science. 2009; 2(9):932-943.
6. Lokhande CD, Dubal DP, Joo OS. Metal oxide thin film based supercapacitors. Current Applied Physics. 2011; 11(3):255-270.
7. Mastragostino M, Arbizzani C, Soavi F. Polymer-based supercapacitors. J Power Sources 2001; 97-98(3):812-815.
8. Bi R-R, Wu X-L, Cao F-F, Jiang L-Y, Guo Y-G, Wan L-J *et al.* Highly Dispersed RuO_2 Nanoparticles on Carbon Nanotubes: Facile Synthesis and Enhanced Supercapacitance Performance. Journal of Physical Chemistry C. 2010; 114(6):2448-2451.
9. Meher SK, Justin P, Rao GR. Microwave-Mediated Synthesis for Improved Morphology and Pseudocapacitance Performance of Nickel Oxide. Acs Applied Materials & Interfaces. 2011; 3(6):2063-2073.
10. Xia X-h, Tu J-p, Mai Y-j, Wang X-l, Gu C-d, Zhao X-b *et al.* Self-supported hydrothermal synthesized hollow Co_3O_4 nanowire arrays with high supercapacitor capacitance. J Mater Chem. 2011; 21(25):9319-9325.
11. Wee G, Soh HZ, Cheah YL, Mhaisalkar SG, Srinivasan M. Synthesis and electrochemical properties of electrospun V_2O_5 nanofibers as supercapacitor electrodes. J Mater Chem. 2010; 20(32):6720-6725.
12. Zhu M, Wang Y, Meng D, Qin X, Diao G. Hydrothermal Synthesis of Hematite Nanoparticles and Their

Electrochemical Properties. Journal of Physical Chemistry C. 2012; 116(30):16276-16285.
13. Yang YH, Zhu J, Shi W, Zhou J, Gong DC, Gu SZ *et al*. 3D nanoporous $ZnWO_4$ nanoparticles with excellent electrochemical performances for supercapacitors. Mater Lett. 2016; 177:34-38.
14. Chen S, Yang G, Jia Y, Zheng H. Three-dimensional $NiCo_2O_4$@$NiWO_4$ core-shell nanowire arrays for high performance supercapacitors. Journal of Materials Chemistry A. 2017; 5(3):1028-1034.
15. Liao S-H, Lu S-Y, Bao S-J, Yu Y-N, Yu L. Electrospinning Synthesis of Porous $CoWO_4$ Nanofibers as an Ultrasensitive, Nonenzymatic, Hydrogen-Peroxide-Sensing Interface with Enhanced Electrocatalysis. Chemelectrochem. 2015; 2(12):2061-2070.
16. Goubard-Bretesche N, Crosnier O, Payen C, Favier F, Brousse T. Nanocrystalline $FeWO_4$ as a pseudocapacitive electrode material for high volumetric energy density supercapacitors operated in an aqueous electrolyte. Electrochem Commun. 2015; 57:61-64.
17. Xu X, Shen J, Li N, Ye M. Facile synthesis of reduced graphene oxide/$CoWO_4$ nanocomposites with enhanced electrochemical performances for supercapacitors. Electrochim Acta. 2014; 150:23-34.
18. Xu X, Pei L, Yang Y, Shen J, Ye M. Facile synthesis of $NiWO_4$/reduced graphene oxide nanocomposite with excellent capacitive performance for supercapacitors. J Alloys Compd. 2016; 654:23-31.
19. Xu X, Yang Y, Wang M, Dong P, Baines R, Shen J *et al*. Straightforward synthesis of hierarchical Co_3O_4@$CoWO_4$/rGO core-shell arrays on Ni as hybrid electrodes for asymmetric supercapacitors. Ceram Int. 2016; 42 (9):10719-10725.
20. Niu L, Li Z, Xu Y, Sun J, Hong W, Liu X *et al*. Simple Synthesis of Amorphous $NiWO_4$ Nanostructure and Its Application as a Novel Cathode Material for Asymmetric Supercapacitors. Acs Applied Materials & Interfaces. 2013; 5(16):8044-8052.
21. Wang Y, Shen C, Niu L, Sun Z, Ruan F, Xu M *et al*. High rate capability of mesoporous $NiWO_4$-$CoWO_4$ nanocomposite as a positive material for hybrid supercapacitor. Mater Chem Phys. 2016; 182:394-401.
22. Xing X, Gui Y, Zhang G, Song C. $CoWO_4$ nanoparticles prepared by two methods displaying different structures and supercapacitive performances. Electrochim Acta. 2015; 157:15-22
23. El-Sheikh SM, Rashad MM. Novel Synthesis of Cobalt Nickel Tungstate Nanopowders and its Photocatalytic Application. J Cluster Sci. 2015; 26(3):743-757.
24. Brown RG, Ross SD. Forbidden transitions in the infra-red spectra of tetrahedral anions V: The infra-red spectra of langbeinites. Spectrochimica Acta Part a Molecular Spectroscopy. 1970; 26(5):1149-1153.
25. Mancheva MN, Iordanova RS, Klissurski DG, Tyuliev GT, Kunev BN. Direct mechanochemical synthesis of nanocrystalline $NiWO_4$. J Physical Chem C. 2007; 111(3):1101-1104.
26. Zhang J, Zhao XS. On the Configuration of Supercapacitors for Maximizing Electrochemical Performance. Chemsuschem. 2012; 5(5):818-841.
27. Wang G, Zhang L, Zhang J. A review of electrode materials for electrochemical supercapacitors. Chem Soc Rev. 2012; 41(2):797-828.
28. Xu X, Gao J, Huang G, Qiu H, Wang Z, Wu J *et al*. Fabrication of $CoWO_4$@$NiWO_4$ nanocomposites with good supercapacitve performances. Electrochim Acta. 2015; 174:837-845.
29. Yuan C, Zhang X, Su L, Gao B, Shen L. Facile synthesis and self-assembly of hierarchical porous NiO nano/micro spherical superstructures for high performance supercapacitors. J Mater Chem. 2009; 19(32):5772-5777.
30. Ji Z, Shen X, Zhou H, Chen K. Facile synthesis of reduced graphene oxide/CeO_2 nanocomposites and their application in supercapacitors. Ceram Int. 2015; 41 (7):8710-8716.
31. Liu M-C, Kong L-B, Lu C, Li X-M, Luo Y-C, Kang L. A Sol-Gel Process for Fabrication of NiO/$NiCo_2O_4$/Co_3O_4 Composite with Improved Electrochemical Behavior for Electrochemical Capacitors. Acs Applied Materials & Interfaces. 2012; 4(9):4631-4636.
32. Kong L-B, Lang J-W, Liu M, Luo Y-C, Kang L. Facile approach to prepare loose-packed cobalt hydroxide nano-flakes materials for electrochemical capacitors. J Power Sources. 2009; 194 (2):1194-1201.
33. Adib K, Rahimi-Nasrabadi M, Rezvani Z, Pourmortazavi SM, Ahmadi F, Naderi HR *et al*. Facile chemical synthesis of cobalt tungstates nanoparticles as high performance supercapacitor. Journal of Materials Science-Materials in Electronics. 2016; 27(5):4541-4550.
34. Meng XY, Feng MG, Zhang H, Ma ZG, Zhang CM. Solvothermal synthesis of cobalt/nickel layered double hydroxides for energy storage devices. J Alloys Compd. 2017; 695:3522-3529.
35. Kaempgen M, Chan CK, Ma J, Cui Y, Gruner G. Printable Thin Film Supercapacitors Using Single-Walled Carbon Nanotubes. Nano Lett. 2009; 9 (5):1872-1876.
36. Yu X, Lu B, Xu Z. Super Long-Life Supercapacitors Based on the Construction of Nanohoneycomb- like Strongly Coupled $CoMoO_4$-3D Graphene Hybrid Electrodes (vol 2, pg 1044, 2014). Adv Mater. 2014; 26(7):990-990.
37. Ma G, Zhang Z, Sun K, Feng E, Peng H, Zhou X *et al*. High-performance aqueous asymmetric supercapacitor based on $K_{0.3}WO_3$ nanorods and nitrogen-doped porous carbon. J Power Sources. 2016; 330:219-230.